Dominant eukaryotic export production during ocean anoxic events reflects the importance of recycled NH_4^+

Meytal B. Higgins[a,b,1], Rebecca S. Robinson[c], Jonathan M. Husson[a,b], Susan J. Carter[a], and Ann Pearson[a,1]

[a]Department of Earth and Planetary Sciences, Harvard University, Cambridge, MA 02138; [b]Department of Geosciences, Princeton University, Princeton, NJ 08544; and [c]Graduate School of Oceanography, University of Rhode Island, Narragansett, RI 02882

Edited by Donald E. Canfield, University of Southern Denmark, Odense M., Denmark, and approved December 23, 2011 (received for review March 17, 2011)

The Mesozoic is marked by several widespread occurrences of intense organic matter burial. Sediments from the largest of these events, the Cenomanian–Turonian Oceanic Anoxic Event (OAE 2) are characterized by lower nitrogen isotope ratios than are seen in modern marine settings. It has remained a challenge to describe a nitrogen cycle that could achieve such isotopic depletion. Here we use nitrogen-isotope ratios of porphyrins to show that eukaryotes contributed the quantitative majority of export production throughout OAE 2, whereas cyanobacteria contributed on average approximately 20%. Such data require that any explanation for the OAE nitrogen cycle and its isotopic values be consistent with a eukaryote-dominated ecosystem. Our results agree with models that suggest the OAEs were high-productivity events, supported by vigorous upwelling. Upwelling of anoxic deep waters would have supplied reduced N species (i.e., NH_4^+) to primary producers. We propose that new production during OAE 2 primarily was driven by direct NH_4^+-assimilation supplemented by diazotrophy, whereas chemocline denitrification and anammox quantitatively consumed NO_3^- and NO_2^-. A marine nitrogen reservoir dominated by NH_4^+, in combination with known kinetic isotope effects, could lead to eukaryotic biomass depleted in ^{15}N.

biomarkers | nitrogen fixation | stable isotopes | paleoceanography

Mid-Cretaceous episodes of deposition of organic-rich sediments in the proto-Atlantic and Western Tethys basins known as Oceanic Anoxic Events (OAEs) (1) are attributed to high productivity and/or enhanced organic-matter preservation resulting from increases in nutrient supply and/or decreases in the ventilation of deep waters (2–6). Because OAEs are thought to be associated with enhanced CO_2 outgassing during emplacement of large igneous provinces (7, 8), understanding the feedbacks between CO_2, anoxia, and nutrient availability may help us understand better the effects of anthropogenic climate change on ocean circulation, oxygen balance, and marine ecology (9).

Basinal anoxia during OAEs would have promoted loss of fixed nitrogen through the processes of denitrification and anammox. The resulting nitrogen deficits in waters returning to the surface via upwelling would have been amended by nitrogen-fixing cyanobacteria, assuming iron and other micronutrients were adequately available (10). Indeed, enhancement of cyanobacterial production during many episodes of ocean anoxia has been proposed based on increased burial of 2-methylhopanoids (11–13), as these compounds are thought to be markers for cyanobacteria (14). Because such biomarker indices are only qualitative indicators of change and cannot provide quantitative estimates of export flux, complementary data generally include isotope ratios of total sedimentary nitrogen ($\delta^{15}N_{TN}$) (11, 15–17), as diazotrophy also affects the nitrogen isotopic budget of the ocean (18–20).

The modern ocean has several localized regions of anoxia, and in these regions, values of $\delta^{15}N_{TN}$ generally are higher than the present deep-water average $\delta^{15}N_{NO_3^-}$ value of +5‰ because of the isotopic fractionation of denitrification expressed in the water column (19, 21, 22). In contrast, sediments from OAE 2 record striking nitrogen isotopic depletion. They are characterized by values of $\delta^{15}N_{TN}$ consistently <−1‰, and often <−3‰ (11, 16, 17, 23). Expression of these negative values of $\delta^{15}N_{TN}$ varies consistently by depositional location, with the average value of $\delta^{15}N_{TN}$ for OAE 2 horizons of the Bonarelli section (Gubbio and Furlo, Italy) being −3.3‰ and the South Ferriby formation (England) being −2.8‰ (16); whereas the average value for the South Atlantic is −1.9‰ (23), for the proto-North Atlantic is −1.8‰ (11, 17, this work), and for the Tarfaya Basin, Morocco is −1.7‰ (between 45–60 m in section) (16). Such differences thus reflect regional heterogeneity of water masses, phototroph ecology, and/or nutrient biogeochemistry; and it has been suggested that patterns of intrabasinal upwelling intensity and nutrient concentrations correspond directly to regional patterns of sedimentation (8, 23, 24).

When viewed alongside the elevated 2-methylhopanoid ratios, negative values of $\delta^{15}N$ have been interpreted as evidence for diazotrophic rebalancing of the nitrogen budget and cyanobacterial dominance of the nitrogen supply for new (export) primary production (6, 11, 15, 25, 26). However, the minimum value of $\delta^{15}N$ for the biomass of marine diazotrophs ($\delta^{15}N_{diazo}$) should be on average approximately −1.3‰, based on the fractionation associated with nitrogenase (ε_{fix} = 0-2‰) and the $\delta^{15}N$ value of dissolved N_2 in seawater (approximately +0.7‰). This number is supported by data that consistently show N-fixing cyanobacteria to have values of $\delta^{15}N_{diazo}$ between 0.5‰ and −2‰ (average -1.4 ± 0.9‰) (25, 27–35). Reports of values significantly <−2‰ are from a cultured *Trichodesmium* sp. (−3.5‰) that was more negative than field samples collected in situ by the same investigators (32) and from experiments on N_2-sparged *Anabaena* spp. (−2.4‰) grown in an artificial-seawater medium (ASP-2) that also contained NH_4^+ (31). Non-N_2-derived N in the culture media may explain these outliers. Given the likelihood that in situ values of $\delta^{15}N_{diazo}$ would average approximately −1‰, the prevalence of sedimentary values lower than −2‰ in many OAE sections cannot be explained solely by N supplied via N fixation. These patterns require that additional N-cycling processes be invoked to explain the source of nitrogen driving primary production during OAEs.

Nitrogen Isotopic Records of Sediments, Porphyrins, and Kerogen

Chlorophyll-derived sedimentary porphyrins can be used to generate records of $\delta^{15}N$ values of eukaryotic and prokaryotic phytoplankton that are unaffected by diagenesis (36, 37), as well as to estimate the contribution of cyanobacteria to burial flux (38). We examined nitrogen cycling during OAE 2 using measurements of coeval bulk and porphyrin nitrogen isotopes in sediments from

Author contributions: M.B.H., R.S.R., and A.P. designed research; M.B.H., R.S.R., J.M.H., S.J.C., and A.P. performed research; M.B.H., R.S.R., and A.P. analyzed data; and M.B.H. and A.P. wrote the paper.

The authors declare no conflict of interest.

This article is a PNAS Direct Submission.

[1]To whom correspondence may be addressed. E-mail: pearson@eps.harvard.edu or meytal@post.harvard.edu.

This article contains supporting information online at www.pnas.org/lookup/suppl/doi:10.1073/pnas.1104313109/-/DCSupplemental.

the Ocean Drilling Program Leg 207, Site 1258A (Demerara Rise). A well-defined positive carbon isotope excursion in this section is contained within the high total organic carbon (TOC) interval commonly associated with the OAE (39) (Fig. 1*A*). Values of $\delta^{15}N_{TN}$ (Fig. 1*B*) from before the OAE through the first two-thirds of the OAE (428.5–423 m composite depth; mcd) decrease from approximately −0.1‰ to approximately −1.4‰ and fluctuate with greater variance than in the middle and top intervals ($p < 0.05$). The middle of the analyzed section (423 to 419.5 mcd), which spans the end of the OAE as defined by $\delta^{13}C_{org}$, is characterized by stable $\delta^{15}N_{TN}$ values of -2.1 ± 0.3‰. The top section (419.5 to 415.5 mcd) is characterized by an increase in $\delta^{15}N_{TN}$ values, returning to −0.7‰ in the uppermost samples. All of these values are lower than the $\delta^{15}N$ minima that are observed in modern sediments, even in regions underlying zones of water-column anoxia or intense nitrogen fixation (40, 41). Because diagenesis and interstitial NH_4^+ in clays can shift values of $\delta^{15}N_{TN}$ (18, 42), we also measured $\delta^{15}N$ values of kerogen. They show an average negative offset of −0.4‰ relative to bulk sediment (Fig. 1*B*), suggesting the original primary producers had even lower $\delta^{15}N$ values than what remains recorded by values of $\delta^{15}N_{TN}$.

Porphyrin values of $\delta^{15}N$ ($\delta^{15}N_{por}$) also show patterns that are similar to bulk N isotopes, although they exhibit more scatter than the $\delta^{15}N_{TN}$ and $\delta^{15}N_{kerogen}$ values. The large error ranges are due to full propagation of analytical uncertainty associated with preparation and analysis by the denitrifier method (43). To overcome the scatter, we plotted 3-, 5-, and 9-point moving averages (Fig. 1*C*). These different resolutions all show similar patterns, indicating that temporal trends in the results are not sensitive to the degree of smoothing and are not dependent on data density. The data are spaced relatively uniformly (0.5 m), although sampling resolution is higher in some horizons surrounding the excursion interval, from 421.9 to 427.5 mcd (0.2 m). The duration of OAE 2 has been estimated to be approximately 400–800 ka (44, 45), corresponding to sampling resolution for the porphyrin data of approximately 20,000–100,000 y per sample, or significantly longer than present-day estimates of N residence time in the ocean (2,000–5,000 y; ref. 9). Trends observed in the smoothed data thus reflect persistent, potentially steady-state perturbations of the marine N cycle. The top and bottom sections of the core have identical values of $\delta^{15}N_{por}$: -5.6 ± 0.7‰ above 419.5 mcd and -5.4 ± 0.7‰ below 423 mcd. However, between 423 and 419.5 mcd, values of $\delta^{15}N_{por}$ average -6.4 ± 0.6‰ and decrease sharply to −7.5‰ approaching and just after the termination of the OAE. This shift correlates with the phasing observed for $\delta^{15}N_{TN}$ and $\delta^{15}N_{kerogen}$, but in both cases the N isotopes lag the excursion observed in $\delta^{13}C_{TOC}$.

The ε_{por} Proxy for Eukaryotic vs. Cyanobacterial Burial

The relative fraction of eukaryotic vs. cyanobacterial export production can be estimated from $\delta^{15}N$ values of porphyrins and their associated sediments. In previous work we examined the biochemical and physiological basis for fractionation of nitrogen isotopes between biomass and chloropigments (38). The offset, known as ε_{por} ($\varepsilon_{por} = \delta^{15}N_{TN} - \delta^{15}N_{por}$), differs systematically between eukaryotes and cyanobacteria. Values of ε_{por} for eukaryotes are around 5 ± 2‰; i.e., chlorophyll 5‰ more depleted in ^{15}N than biomass (33, 38, 46). In contrast, cyanobacteria have values of ε_{por} between 0 and −10‰ (i.e., chlorophyll equal to or up to 10‰ *enriched* in ^{15}N relative to biomass). One example of a value of ε_{por} near −10‰ had been observed previously for *Anabaena cylindrica* (33). To expand on this finding, we recently reported data showing that among the seven species of cyanobacteria tested to date, freshwater ecotypes cluster around the $\varepsilon_{por} = -10 \pm 2$‰ endmember, whereas marine ecotypes cluster around the $\varepsilon_{por} = 0 \pm 2$‰ endmember (38).

Because ε_{por} reflects intracellular partitioning of N isotopes downstream of the amino acid glutamate, it is independent of the nitrogen substrate utilized by the organism (N_2, NO_3^-, or NH_4^+; ref. 38). Thus, we proposed that ε_{por} would be an excellent proxy for calculating the relative contributions of eukaryotes and cyanobacteria to marine export production. Measured values of ε_{por} would be 5 ± 2‰ in a 100% eukaryotic system and would be 0 ± 2‰ in a 100% marine cyanobacterial system, regardless of the proportion of diazotrophic species among the latter (not all marine cyanobacteria are diazotrophs). Moreover, influx of terrigenous biomass and/or cyanobacteria from fresh waters would lead to values of $\varepsilon_{por} < 0$‰. Indeed, to date the only in situ value of cyanobacterial ε_{por} from the environment is from a freshwater lake in Japan in which ε_{por} was determined to be −13 to −16‰ (47).

At Site 1258A the observed value of ε_{por} throughout the section averages 4.3 ± 0.8‰ (if calculated vs. $\delta^{15}N_{TN}$) or

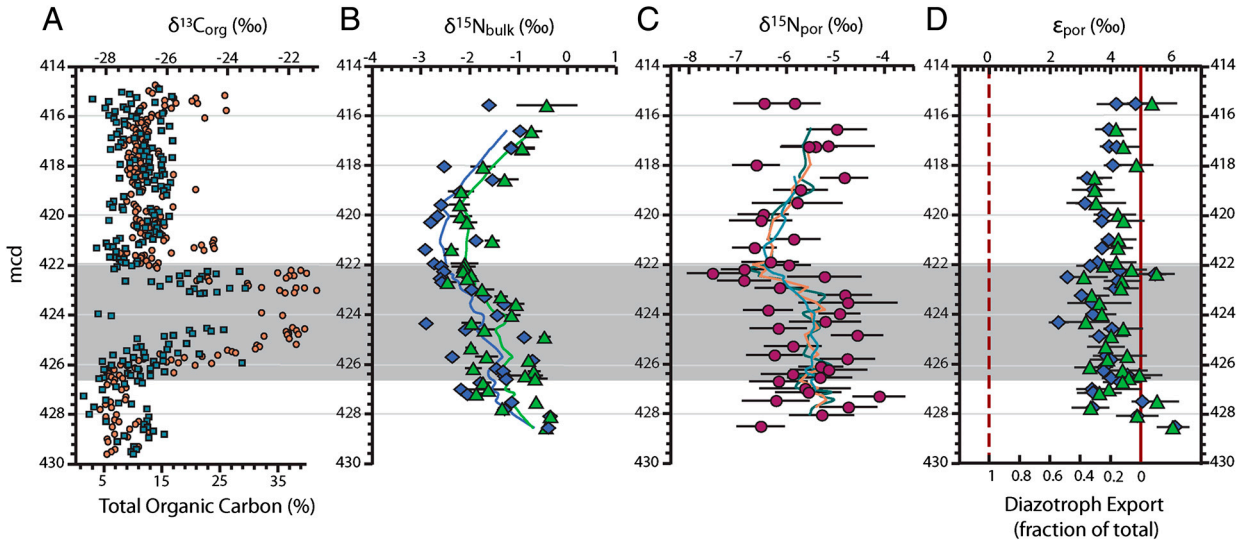

Fig. 1. Elemental and isotopic data for site 1258A. The shaded bar represents the $\delta^{13}C_{org}$ excursion interval that defines the OAE. (*A*) %TOC (squares) and $\delta^{13}C_{org}$ (circles) from (39). (*B*) $\delta^{15}N$ values of bulk sediment (triangles) and kerogen (diamonds), and their 1-*m* averaged trends. (*C*) Porphyrin $\delta^{15}N$ values, and their 3- (green), 5- (tan), and 9- (blue) point averaged trends. (*D*) The isotopic offset ε_{por} between bulk sediment and porphyrins (triangles), and kerogen and porphyrins (diamonds), as well as the corresponding fraction of cyanobacterial export based on the endmember values described in the text. The solid vertical line represents a typical algal value of ε_{por}, and the dotted vertical line represents a marine cyanobacterial value of ε_{por} (38). All error bars represent 1σ, and preparative and analytical errors are compounded when possible. Raw data are shown in Table S1.

$4.0 \pm 0.8‰$ (if calculated vs. $\delta^{15}N_{kerogen}$) (Fig. 1*D*). The values of ε_{por} reach minima—reflecting maximum burial of cyanobacterial biomass—toward the end of the OAE. There appears to be a qualitative trend of decreasing magnitude of ε_{por} from the beginning of the OAE until approximately 1 mcd below the termination. At this point, ε_{por} increases and fluctuates repeatedly until approximately 4 mcd after termination of the OAE, after which ε_{por} then returns to the starting value near 5‰. This again shows that changes in nitrogen cycle processes are out of phase with the changes in the carbon cycle that define the OAE. Such differences may be expected: in multiple OAE 2 sections the local primary productivity is known to be variable within the overall record of the OAE as defined by $\delta^{13}C$ values (24, 48).

If we assume that only eukaryotic algae and marine cyanobacteria contribute significantly to the burial flux of photosynthetic pigments (i.e., eliminating the possibility of freshwater cyanobacteria), a value of ε_{por} consistently >4‰ during the OAE indicates that the export flux remained on average ≥80% eukaryotic throughout the event. In contrast with previous interpretations invoking N fixers as the primary source of nutrient N (11, 15, 26), these results indicate that the abundance of cyanobacteria contributing directly to export production during OAE 2 was not large; and it suggests that another N source would have been required to sustain such high rates of eukaryotic export production. However, the data for ε_{por} are consistent with a large *relative* change in the cyanobacterial population, as observed values of ε_{por} approximately 4‰ within the OAE indicate approximately 20% cyanobacterial biomass, whereas pre- and post-OAE values of ε_{por} nearer 5‰ indicate less burial of cyanobacterial biomass (certainly <5–10%). The ε_{por} data thus indicate at minimum a doubling to quadrupling of cyanobacterial production, but within a system consistently and overwhelmingly dominated by eukaryotic primary producers. If Site 1258A is representative of OAE 2 in general, the widespread negative values of sedimentary $\delta^{15}N_{TN}$ throughout OAE 2 deposits must be attributed to burial of eukaryotes having significant ^{15}N-depletion in their biomass.

Nitrogen Cycle in Anoxic Oceans: A Paradox of Nitrification and Denitrification

A modest increase in cyanobacterial production is consistent with expected changes to the nitrogen cycle. During OAE 2, anoxic deep waters of the proto-Atlantic and Western Tethys would have contained nitrogen predominantly in the form of NH_4^+. Upwelling rates were high (8), and NH_4^+ upwelled into oxic surface waters either was assimilated by phytoplankton or oxidized to NO_2^- and/or NO_3^-. Reducing conditions impinging on the photic zone likely meant that a greater fraction of this NO_2^- and NO_3^- subsequently was reduced to N_2 via denitrification and anammox, causing a modestly greater fixed-nitrogen deficit. Such widespread N deficits suggest it is unlikely that negative values of $\delta^{15}N_{TN}$ in sediments of OAE 2 could be due to the expression of isotopic discrimination during nutrient uptake, which occurs for eukaryotes only in nutrient-replete systems in which the nitrogen supply is in excess of biological demand (49, 50). The extent to which fixed N was used to completion in OAE 2 surface waters would have determined the ecological niche for N-fixing cyanobacteria, either as free-living cells or as symbionts; but the overall system was N limited, as generally is the case in the marine photic zone (10). Complete utilization of the available nutrient N implies that the total flux must have been isotopically negative.

A deficit in fixed N during OAEs is not surprising, as anoxia promotes denitrification. What may be surprising is that the deficit was not larger. We suggest that counterintuitively, rates of denitrification may decrease under conditions of extreme basin-wide anoxia. Denitrification and anammox depend on sufficient availability of NO_3^- and NO_2^-. Because these oxidized N species are produced aerobically, extreme oxygen limitation in the water-column may decrease their rate of formation, leaving a greater fraction of remineralized organic nitrogen to cycle throughout these regionally isolated basins and reenter the photic zone as NH_4^+. This in turn would limit the need for compensating N fixation. Evidence for photic-zone sulfide oxidation during OAEs suggests that NO_3^- indeed was completely absent beneath the photic zone, at least episodically (5, 51), and that fixed N in these deep waters would have remained in reduced form. We propose that the values of $\delta^{15}N_{TN} < -2‰$ found in OAE sediments reflect severe diminishment of the deep-water NO_3^- component of the marine N cycle, implying that the deep ocean was a reservoir of NH_4^+. Upwelled NH_4^+, rather than newly fixed N, was the main N source for primary production. Chemocline impingement on the photic zone would have driven nitrification, denitrification, and anammox into competition with NH_4^+-assimilation. The balance between these processes—which varied regionally—would have set the loss rate of N from the ocean and the compensatory rates of N fixation.

To explain the observed values of $\delta^{15}N_{TN}$, isotopic mass balance would then require that the newly fixed N ($\delta^{15}N_{diazo} = 0$ to $-2‰$), plus the upwelled NH_4^+ supply, together can yield new production that has values of $\delta^{15}N < -2‰$ (e.g., Bonarelli and South Ferriby sections; ref. 16). This is different from a modern-ocean scenario, in which denitrification associated with the spreading of anoxic zones leads to progressively higher (positive) values of $\delta^{15}N_{NO_3^-}$ that are then propagated to $\delta^{15}N_{TN}$ (21, 22). The modern-ocean endmembers are thus near-zero (diazotrophs) and more positive (nitrate assimilation and/or recycling), whereas the OAE endmembers must be near-zero (diazotrophs) and more negative (NH_4^+ assimilation and recycling). Although required to explain the data, such a scenario is far from intuitive: it requires that the fixed N lost from the ocean by the processes of denitrification plus anammox have a net positive value of $\delta^{15}N$. Below we explore how such a system might be possible.

NH_4^+-Upwelling Model

To yield a marine system in which the burial flux of $\delta^{15}N_{TN}$ has a negative value, we assume that NO_3^- (and NO_2^-) are produced only in the aerobic photic zone and are reduced quantitatively to N_2 in the chemocline by denitrification and/or anammox. This loss is analogous isotopically to sedimentary denitrification in the modern ocean, which is considered to impart zero fractionation because it proceeds to completion, and by mass balance, $\delta^{15}N_{inputs} = \delta^{15}N_{outputs}$ (19).

The following additional conditions then would be sufficient to achieve a denitrifying flux of N_2 that is net isotopically positive. To yield surface waters in which NH_4^+ and N_2 are the most important bioavailable sources of N, we assume that nitrification of the upwelling flux to NO_3^- followed by phytoplanktonic assimilation is much less significant than direct assimilation of concomitant upwelling NH_4^+. Where NH_4^+ is available, NO_3^- is a less favorable nutrient for phytoplankton growth due to the higher energetic costs associated with its reduction (52). Nitrite generally is not believed to be an important source of nutrient N (53), and thus we assume it also is removed by denitrification or, more likely, by anammox. The dominant fractionations and fluxes in the N cycle are then ε_{fix} and φ_{fix} (N_2 fixation), ε_1 and φ_1 (NH_4^+-assimilation), and ε_2 and φ_2 (ammonium oxidation, $NH_4^+ \rightarrow NO_2^-$), whereas the burial flux is small relative to these internal cycles (Fig. 2*A*). We also specify the flux associated with remineralization of sinking phytoplankton N (φ_3), and assume no fractionation for this process. As stated above, all oxidations and reductions downstream of φ_2 are quantitative and do not impart further fractionation.

In N-limited surface waters, new production reflects the isotopic signature of the integrated nitrogen budget. The resulting value of $\delta^{15}N_{TN}$ will reflect a weighted average of the $\delta^{15}N$ values of diazotrophic cyanobacteria (δ_{diazo}) and of NH_4^+-consuming phytoplankton (δ_{phyto}). The former will be equal to $\delta^{15}N_{N2(aq)}$

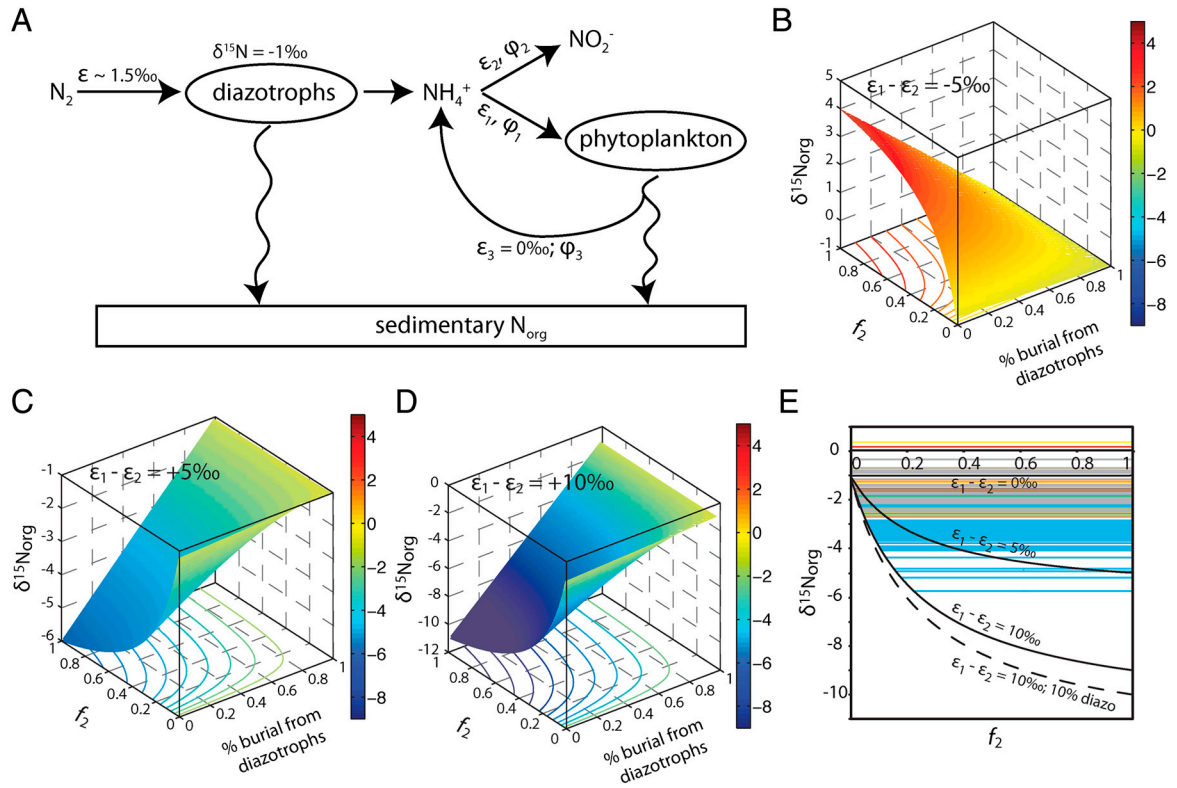

Fig. 2. Conceptual model for sedimentary values of $\delta^{15}N_{TN}$ in an ocean in which NH_4^+ is the dominant fixed N species. (*A*) System in which the $\delta^{15}N$ values of exported eukaryotic biomass depend on the fractional fluxes to ammonium assimilation (φ_1), oxidation (φ_2), and recycling (φ_3), as well as the difference between the associated fractionation factors ε_1 and ε_2. (*B–D*) Calculated $\delta^{15}N$ values of sedimentary organic matter as a function of percent export from diazotrophs and fractional fluxes φ_1 and φ_2 for three sets of fractionation factors: (*B*) $\varepsilon_1 - \varepsilon_2 = -5‰$; (*C*) $\varepsilon_1 - \varepsilon_2 = 5‰$; (*D*) $\varepsilon_1 - \varepsilon_2 = 10‰$. (*E*) Data for $\delta^{15}N_{TN}$ for OAE 2 from the literature [*11* (red); *16* (blue, Italy; green, England); *17* (yellow); *23* (orange), and this study (gray)], plotted relative to the range of paired values of ε_1 and ε_2 solved with the model, assuming 20% export of diazotrophic biomass (solid lines), as well as an $\varepsilon_1/\varepsilon_2$ offset of 10‰ assuming 10% export of diazotrophic biomass (dashed line).

minus ε_{fix}, whereas the latter will be equal to the $\delta^{15}N$ value of their NH_4^+ source minus a fractionation factor ε_1. Isotopic mass balance dictates that the source $\delta^{15}N_{NH_4^+}$ is set by the relative flux of NH_4^+ that is utilized (φ_1) vs. nitrified (φ_2), as well as the flux (φ_3) that returns remineralized NH_4^+ to the surface via upwelling. Ratios of these fluxes, the fractionations associated with NH_4^+ utilization and oxidation (ε_1 and ε_2, respectively), and the value of δ_{diazo}, together set $\delta_{NH_4^+}$:

$$\delta_{NH_4^+} = \delta_{diaz} + \frac{\varphi_1 - \varphi_3}{\varphi_1 + \varphi_2 - \varphi_3} * \varepsilon_1 + \frac{\varphi_2}{\varphi_1 + \varphi_2 - \varphi_3} * \varepsilon_2.$$

Assuming $\delta_{diazo} = -1‰$ and substituting $\delta_{phyto} = \delta_{NH_4^+} - \varepsilon_1$ and $\delta_{NO_2^-} = \delta_{NH_4^+} - \varepsilon_2$ enables the system to be solved for a range of combinations of ε_1 and ε_2 (full derivation in *SI Text*). This model generates negative values for δ_{phyto} when $\varepsilon_1 > \varepsilon_2$, and it produces an ocean system in which the major reservoir of dissolved inorganic nitrogen (DIN) accumulates as ^{15}N-depleted NH_4^+.

Biomass having a negative value of $\delta^{15}N$ results from the co-occurrence of ammonium oxidation and ammonium assimilation in the photic zone, the competing effects of fractionations associated with these processes on a single NH_4^+ pool, and the upwelling of recycled, ^{15}N-depleted NH_4^+. Both assimilation and oxidation fractionate such that their products are more ^{15}N-depleted than the source NH_4^+, and therefore the NH_4^+ pool in surface waters becomes more ^{15}N-enriched as it is consumed. If the fractionation associated with NH_4^+ assimilation exceeds the enrichment of the NH_4^+ pool that is caused by nitrification/denitrification (i.e., $\varepsilon_1 > \varepsilon_2$), the resulting biomass (φ_1) is isotopically negative. Regenerated NH_4^+ in deep waters isotopically resembles the sinking biomass from which it is remineralized. As this NH_4^+ upwells into the photic zone, it again becomes ^{15}N-enriched and the system maintains steady-state.

The resulting value for total buried organic matter ($\delta^{15}N_{TN}$) is tempered by the percent contribution of diazotrophic biomass (Fig. 2 *B–D*) such that values of $\delta^{15}N_{TN}$ approach $-1‰$ when there is greater burial of diazotrophs, but decrease as the ratio φ_2/φ_1 increases and diazotrophic burial decreases. This is consistent with records showing the most negative values of $\delta^{15}N_{TN}$ in pelagic locations with lesser apparent bacterial biomass burial (16) and more positive values of $\delta^{15}N_{TN}$ in epicontinental environments with higher apparent bacterial flux (16).

The model thus depends on the relative magnitudes of ε_1 and ε_2 compared to the N deficit and resulting diazotrophic contribution. It is possible that the fractionation associated with NH_4^+-assimilation (ε_1) by the enzyme glutamine synthetase (GS) may exceed that of NH_4^+-oxidation (ε_2) by the enzyme ammonium monooxygenase (AMO) under some circumstances. The observed value of ε_1 (4–27‰) will depend on NH_4^+ concentration, with larger fractionations expressed under NH_4^+-rich conditions (54). In the modern ocean, NH_4^+ concentrations are low and ε_1 is confined to the lower end of this range. Under the NH_4^+-replete conditions that we propose for OAE 2, assimilation using different enzymatic controls may lead to expression of ε_1 with a larger magnitude, although to date very little information is available about fractionation during NH_4^+ assimilation by natural planktonic assemblages (55).

The value of ε_2 also remains poorly constrained. The relative fraction of aerobic ammonia oxidation by archaea vs. bacteria during OAE 2 is not known, but $\delta^{13}C$ and archaeal biomarker data measured in black shales deposited during the Albian OAE1b (approximately 112 Ma) suggest that Crenarchaeota

(now called Thaumarchaeota; ref. 56) that are believed to be responsible for most ammonium oxidation in the modern ocean (57), were abundant in the Cretaceous (58). Values of ε_2 for bacterial AMO are approximately 14–38‰, for a variety of species grown on 1–2 mM NH_4^+ (59). Recent measurements of isotope effects associated with archaeal ammonia oxidation show a similar range of values, from 10–37‰ (60). In all cases, the relative contributions of fractionations associated with transport of NH_4^+ or diffusion of NH_3 through membranes and equilibrium of NH_4^+/NH_3 are uncertain. It is thus difficult to extrapolate these cultures to natural systems, except to suggest that bacterial and archaeal AMO results are similar.

If ε_1 was large due to elevated NH_4^+ concentrations (54) upwelling to the base of the photic zone from a large, deep NH_4^+ pool, the condition of $\varepsilon_1 > \varepsilon_2$ could be met. For example, if $\varepsilon_2 =$ 22‰ (average archaeal value) and $\varepsilon_1 = 27$‰ (maximum enzymatic effect on NH_4^+-assimilation), then $\varepsilon_1 - \varepsilon_2 = 5$‰. This results in values of $\delta^{15}N_{TN}$ for export production that will be <-2‰ (Fig. 2*C*) if NH_4^+ oxidation consumes at least one-tenth of the upwelling NH_4^+ flux ($\varphi_2 > 0.1$) and the burial contribution of diazotrophs is 20%, the upper limit based on our data for ε_{por}. Other versions of the model that impose larger differences between ε_1 and ε_2 (e.g., $\varepsilon_1 - \varepsilon_2 = 10$‰, Fig. 2*D*) also are compatible with some of the data from OAE 2, in particular a few of the very negative values of $\delta^{15}N_{TN}$ for the sections from Italy and England (Fig. 2 *D* and *E*) (16). Analogous models with $\varepsilon_1 < \varepsilon_2$ can produce only positive values of $\delta^{15}N_{TN}$, as would be seen in the modern ocean (Fig. 2*B*). Using our conceptual model, most data for $\delta^{15}N_{TN}$ compiled from OAE 2 (11, 16, 17, 23, this paper) fall within isotope space corresponding to ranges of $\varepsilon_1 - \varepsilon_2 =$ 5‰ (Fig. 2*E*).

We further tested the plausibility of our conceptual framework using a simplified steady-state model that calculates $\delta^{15}N$ values of biomass N, NH_4^+, NO_2^-, and NO_3^- in a two-box (surface and deep) ocean. The model was optimized to reproduce known modern values using estimates of fluxes and fractionation factors from the literature. To run the model subsequently for the OAE, we modified nitrogen-redox partitioning (more NH_4^+, less NO_3^-) and changed the magnitude of associated fluxes proportionally. Rates of upwelling and the total N inventory remained the same in both cases. By changing these parameters, the model generated sedimentary $\delta^{15}N_{TN}$ values of −4.4‰ for the OAE and +4.9‰ for modern sediments. For a complete model description, results, and sensitivity analysis, see *Supplementary Information*.

Implications

Our model implies a widespread and well-mixed "ammonia ocean" for the proto-Atlantic and Western Tethys because it requires a sustained source of upwelling NH_4^+ that can be used for biological assimilation. This can be achieved if nitrate production is limited by severe demands on NO_2^-, possibly through enhanced anammox. In such an ocean, ammonia assimilators and N fixers both could out-compete assimilatory NO_3^- reducers due to the dominance of NH_4^+ and a limited rate of NO_3^- generation. Postulated high rates of upwelling, combined with nutrient trapping under estuarine circulation in the North Atlantic (8), may explain why these negative $\delta^{15}N$ signals are widespread during OAEs, yet are regionally variable (16). The trapping of quantitatively significant levels of NH_4^+ in deep waters during OAEs also helps preserve the total pool of marine N, alleviating the need for excessive rates of nitrogen fixation. Extreme anoxia may therefore exert a natural, negative feedback on the nitrogen cycle by preventing the ocean from denitrifying completely.

Our proposed model for the N cycle during OAE 2 also helps to explain why extreme N isotopic depletion is not seen in modern anoxic basins like the Black Sea and the Cariaco Trench, where $\delta^{15}N$ values of particulate organic nitrogen are >0‰ throughout the water column (41). The nutrient sources and circulation patterns in these two systems are not analogous to anoxic oceans. The Cariaco Trench is a silled basin that receives NO_3^- from the Atlantic, and sedimentary organic nitrogen in the Cariaco basin carries an isotopic signature that reflects a mass balance between Atlantic NO_3^- that has been influenced by N_2 fixation (approximately 3‰) and N_2 (local nitrogen fixation) (61). In the Black Sea, a commonly used analog for anoxic oceans, the supply of N to surface waters is largely sourced from continental rivers, whereas the intense salinity stratification limits the upwelling of deep NH_4^+ and promotes formation of NO_2^- followed by nearly quantitative loss via the anammox process (62). The nutrient N cycle of the modern Black Sea, therefore, primarily is analogous to a large lacustrine system with severe stratification. In contrast, we envision OAE 2 as a time of sustained upwelling.

The ammonia ocean scenario also may help to explain the temporal evolution of N isotope patterns seen in our data. Values of $\delta^{15}N_{por}$ and $\delta^{15}N_{TN}$ are out of phase with carbon isotopes. They do not begin to decrease until the middle of the OAE interval, and their minimum persists past the traditionally defined termination of the event. This phase lag may reflect the balance of oxidants in the marine system. Enhanced burial of organic carbon during OAEs should be associated with accumulation of oxygen in the ocean and atmosphere. This in turn would increase the rates of ammonium oxidation and nitrification, eventually suppressing anammox and allowing NO_3^- to accumulate. Indeed, our predicted values of $\delta^{15}N_{TN}$ decrease as φ_2 increases (Fig. 2 *C*–*E*). The predicted isotopic trajectory, therefore, is that $\delta^{15}N_{TN}$ values will decrease during the early stages of ocean reoxidation. Values of $\delta^{15}N_{TN}$ only would "flip" to positive values when the nitrification flux (φ_2) was sufficiently high to accumulate excess NO_3^-, allowing subsequent denitrification to enrich ^{15}N in the accumulating NO_3^- reservoir. These results highlight the importance and promise of using temporal records of ε_{por} in conjunction with $\delta^{15}N_{TN}$ values to examine both the succession of marine ecosystems and the redox state of the ocean.

In sum, a mid-Cretaceous deep ocean dominated by reduced rather than oxidized nitrogen species, normal rates of ocean circulation (63), and enhanced input of nutrients (5, 6, 8) together could yield negative values of biomass $\delta^{15}N$ and sustain a primary producer community that remained rich in eukaryotes. Although the oxidation state and temperature of OAE oceans was very different from the modern ocean, the persistent dominance of eukaryotes and dependence of primary producers on upwelled nutrients suggests that the balance between gross and net production was not greatly dissimilar from the present-day. Our results imply that additional feedbacks act under oxygen-limited conditions to maintain nitrogen balance, thereby limiting the extent of denitrification and the compensatory expansion of diazotrophy during OAEs.

Materials and Methods

Sediments were obtained from Ocean Drilling Program Leg 207, Site 1258A, from the Demerara Rise, offshore from modern Surinam. Samples spanned 415–428 m composite depth (mcd). Forty samples were analyzed for bulk $\delta^{15}N_{TN}$, $\delta^{15}N_{kerogen}$, and $\delta^{15}N_{por}$ at approximately 0.5-m spacing. Sampling resolution was higher leading into and coming out of the OAE, which spanned approximatley 422–426 mcd (Table S1. Sample preparation and isotopic analysis followed established methods (43); details are given in *SI Text*.

ACKNOWLEDGMENTS. We thank Roger Summons, Carolyn Colonero, Amy Kelly, Noreen Tuross, and Kyle McElhoney for assistance with sample preparation and analysis and machine use. We thank Chris Junium and Julian Sachs for helpful discussions and comments, and Don Canfield, the PNAS editorial staff, and two anonymous reviewers for their valuable input. This work was supported by the National Science Foundation Grant OCE-0825269 (to A.P. and R.S.R.) and by the National Aeronautics and Space Administration Astrobiology Institute and the David and Lucille Packard Foundation (A.P.)

1. Schlanger SO, Jenkyns HC (1976) Cretaceous oceanic anoxic events: Causes and consequences. *Geol Mijnbouw* 55:179–184.
2. Jenkyns HC (1980) Cretaceous anoxic events—from continents to oceans. *J Geol Soc London* 137:171–188.
3. Bralower TJ, Thierstein HR (1987) Organic carbon and metal accumulation rates in Holocene and mid-Cretaceous sediments: Palaeoceanographic significance. *Geol Soc Spec Publ*, pp:345–369.
4. Pedersen TF, Calvert SE (1990) Anoxia vs productivity—what controls the formation of organic carbon-rich sediments and sedimentary rocks. *AAPG Bull* 74:454–466.
5. Kuypers MMM, Pancost RD, Nijenhuis IA, Damste JSS (2002) Enhanced productivity led to increased organic carbon burial in the euxinic North Atlantic basin during the late Cenomanian oceanic anoxic event. *Paleoceanography* 17:3.1–13.
6. Jenkyns HC (2010) Geochemistry of oceanic anoxic events. *Geochem Geophy Geosy* 11:Q03004.
7. Turgeon SC, Creaser RA (2008) Cretaceous oceanic anoxic event 2 triggered by a massive magmatic episode. *Nature* 454:323–329.
8. Alexandre JT, et al. (2010) The mid-Cretaceous North Atlantic nutrient trap: Black shales and OAEs. *Paleoceanography* 25:PA4201.
9. Brandes JA, Devol AH (2002) A global marine-fixed nitrogen isotopic budget: Implications for Holocene nitrogen cycling. *Global Biogeochem Cy* 16:1120.
10. Falkowski PG (1997) Evolution of the nitrogen cycle and its influence on the biological sequestration of CO_2 in the ocean. *Nature* 387:272–275.
11. Kuypers MMM, van Breugel Y, Schouten S, Erba E, Damste JSS (2004) N-2-fixing cyanobacteria supplied nutrient N for Cretaceous oceanic anoxic events. *Geology* 32:853–856.
12. Xie SC, Pancost RD, Yin HF, Wang HM, Evershed RP (2005) Two episodes of microbial change coupled with Permo/Triassic faunal mass extinction. *Nature* 434:494–497.
13. Sepulveda J, et al. (2009) Molecular isotopic evidence of environmental and ecological changes across the Cenomanian–Turonian boundary in the Levant Platform of central Jordan. *Org Geochem* 40:553–568.
14. Summons RE, Jahnke LL, Hope JM, Logan GA (1999) 2-Methylhopanoids as biomarkers for cyanobacterial oxygenic photosynthesis. *Nature* 400:554–557.
15. Ohkouchi N, Kashiyama Y, Kuroda J, Ogawa NO, Kitazato H (2006) The importance of diazotrophic cyanobacteria as primary producers during Cretaceous Oceanic Anoxic Event 2. *Biogeosciences* 3:467–478.
16. Jenkyns HC, Matthews A, Tsikos H, Erel Y (2007) Nitrate reduction, sulfate reduction, and sedimentary iron isotope evolution during the Cenomanian–Turonian oceanic anoxic event. *Paleoceanography* 22:PA3208.
17. Junium CK, Arthur MA (2007) Nitrogen cycling during the cretaceous, Cenomanian–Turonian oceanic anoxic event II. *Geochem Geophy Geosy* 8:Q03002.
18. Altabet MA (1988) Variations in nitrogen isotopic composition between sinking and suspended particles—implications for nitrogen cycling and particle transformation in the open ocean. *Deep-Sea Res* 35:535–554.
19. Deutsch C, Sigman DM, Thunell RC, Meckler AN, Haug GH (2004) Isotopic constraints on glacial/interglacial changes in the oceanic nitrogen budget. *Global Biogeochem Cy* 18:GB4012.
20. Casciotti KL, Glover DM, Trull TW, Davies D (2008) Constraints on nitrogen cycling at the subtropical North Pacific Station ALOHA from isotopic measurements of nitrate and particulate nitrogen. *Deep Sea Res Part 2 Top Stud Oceanogr* 55:1661–1672.
21. Brandes JA, Devol AH, Yoshinari T, Jayakumar DA, Naqvi SWA (1998) Isotopic composition of nitrate in the central Arabian Sea and eastern tropical North Pacific: A tracer for mixing and nitrogen cycles. *Limnol Oceanogr* 43:1680–1689.
22. Ganeshram RS, Pedersen TF, Calvert SE, McNeill GW, Fontugne MR (2000) Glacial-interglacial variability in denitrification in the world's oceans: Causes and consequences. *Paleoceanography* 15:361–376.
23. Rau GH, Arthur MA, Dean WE (1987) $^{15}N/^{14}N$ variations in Cretaceous Atlantic sedimentary sequences: Implications for past changes in marine nitrogen biogeochemistry. *Earth Planet Sci Lett* 82:269–279.
24. Tsikos H, et al. (2004) Carbon-isotope stratigraphy recorded by the Cenomanian–Turonian Oceanic Anoxic Event: Correlation and implications based on three key localities. *J Geo Soc London* 161:711–719.
25. Wada E, Hattori A (1976) Natural abundance of N-15 in particulate organic matter in the North Pacific Ocean. *Geochim Cosmochim Acta* 40:249–251.
26. Kashiyama Y, et al. (2008) Diazotrophic cyanobacteria as the major photoautotrophs during mid-Cretaceous oceanic anoxic events: Nitrogen and carbon isotopic evidence from sedimentary porphyrin. *Org Geochem* 39:532–549.
27. Wada E (1980) Nitrogen isotope fractionation and its significance in biogeochemical processes occurring in marine environments. *Isotope Marine Chemistry*, eds ED Goldberg, Y Horibe, and K Saruhashi (Uchida Rokahuko, Tokyo), pp 375–398.
28. Macko SA, Entzeroth L, Parker PL (1984) Regional differences in nitrogen and carbon isotopes on the continental shelf of the Gulf of Mexico. *Naturwissenschaften* 71:374–375.
29. Minagawa M, Wada E (1984) Stepwise enrichment of N-15 along food chains—further evidence and the relation between $\delta^{15}N$ and animal age. *Geochim Cosmochim Acta* 48:1135–1140.
30. Minagawa M, Wada E (1986) Nitrogen isotope ratios of red tide organisms in the East China Sea—a characterization of biological nitrogen fixation. *Mar Chem* 19:245–259.
31. Macko SA, Fogel ML, Hare PE, Hoering TC (1987) Isotopic fractionation of nitrogen and carbon in the synthesis of amino acids by microorganisms. *Chem Geol* 65(1):79–92.
32. Carpenter EJ, Harvey HR, Fry B, Capone DG (1997) Biogeochemical tracers of the marine cyanobacterium Trichodesmium. *Deep Sea Res Part 1 Oceanogr Res* 44:27–38.
33. Beaumont VI, Jahnke LL, Des Marais DJ (2000) Nitrogen isotopic fractionation in the synthesis of photosynthetic pigments in Rhodobacter capsulatus and Anabaena cylindrica. *Org Geochem* 31:1075–1085.
34. Zerkle AL, Junium CK, Canfield DE, House CH (2008) Production of N-15-depleted biomass during cyanobacterial N-2-fixation at high Fe concentrations. *J Geophys Res Biogeosci* 113:G03014.
35. Bauersachs T, et al. (2009) Nitrogen isotopic fractionation associated with growth on dinitrogen gas and nitrate by cyanobacteria. *Limnol Oceanogr* 54:1403–1411.
36. Sachs JP, Repeta DJ (1999) Oligotrophy and nitrogen fixation during eastern Mediterranean sapropel events. *Science* 286:2485–2488.
37. Higgins MB, Robinson RS, Carter SJ, Pearson A (2010) Evidence from chlorin nitrogen isotopes for alternating nutrient regimes in the Eastern Mediterranean Sea. *Earth Planet Sci Lett* 290:102–107.
38. Higgins MB, et al. (2011) Paleoenvironmental implications of taxonomic variation among $\delta^{15}N$ values of chloropigments. *Geochim Cosmochim Acta*, 75 pp:7351–7363.
39. Erbacher J, Friedrich O, Wilson PA, Birch H, Mutterlose J (2005) Stable organic carbon isotope stratigraphy across Oceanic Anoxic Event 2 of Demerara Rise, western tropical Atlantic. *Geochem Geophy Geosy* 6:Q06010.
40. Bianchi TS, et al. (2000) Cyanobacterial blooms in the Baltic Sea: Natural or human-induced? *Limnol Oceanogr* 45:716–726.
41. Thunell RC, Sigman DM, Muller-Karger F, Astor Y, Varela R (2004) Nitrogen isotope dynamics of the Cariaco Basin, Venezuela. *Global Biogeochem Cy* 18:GB3001.
42. Muller PJ (1977) C-N ratios in Pacific deep sea sediments—effect of inorganic ammonium and organic nitrogen compounds sorbed by clays. *Geochim Cosmochim Acta* 41:765–776.
43. Higgins MB, Robinson RS, Casciotti KL, McIlvin MR, Pearson A (2009) A method for determining the nitrogen isotopic composition of porphyrins. *Anal Chem* 81:184–192.
44. Sageman BB, Meyers SR, Arthur MA (2006) Orbital time scale and new C-isotope record for Cenomanian–Turonian boundary stratotype. *Geology* 34:125–128.
45. Mitchell RN, et al. (2008) Oceanic anoxic cycles? Orbital prelude to the Bonarelli Level (OAE 2). *Earth Planet Sci Lett* 267:1–16.
46. Sachs JP, Repeta DJ, Goericke R (1999) Nitrogen and carbon isotopic ratios of chlorophyll from marine phytoplankton. *Geochim Cosmochim Acta* 63:1431–1441.
47. Katase T, Wada E (1990) Isolation of chlorophyll-a in Microcystis spp. for determination of stable isotopes of carbon and nitrogen, and variation in Suwa Lake. *Bunseki Kagaku* 39:451–456.
48. Kuroda J, Ohkouchi N, Ishii T, Tokuyama H, Taira A (2005) Lamina-scale analysis of sedimentary components in Cretaceous black shales by chemical compositional mapping: Implications for paleoenvironmental changes during the Oceanic Anoxic Events. *Geochim Cosmochim Acta* 69:1479–1494.
49. Altabet MA, Francois R (1994) Sedimentary nitrogen isotopic ratio as a recorder for surface ocean nitrate utilization. *Global Biogeochem Cy* 8:103–116.
50. Waser NA, et al. (1998) Nitrogen isotope fractionation during nitrate, ammonium and urea uptake by marine diatoms and coccolithophores under various conditions of N availability. *Mar Ecol-Prog Ser* 169:29–41.
51. Pancost RD, et al. (2004) Further evidence for the development of photic-zone euxinic conditions during Mesozoic oceanic anoxic events. *J Geol Soc London* 161:353–364.
52. Eppley RW, Coatsworth JL, Solorzano L (1969) Studies of nitrate reductase in marine phytoplankton. *Limnol Oceanogr* 14:194–205.
53. Casciotti KL, McIlvin MR (2007) Isotopic analyses of nitrate and nitrite from reference mixtures and application to Eastern Tropical North Pacific waters. *Mar Chem* 107:184–201.
54. Hoch MP, Fogel ML, Kirchman DL (1992) Isotope fractionation associated with ammonium uptake by a marine bacterium. *Limnol Oceanogr* 37:1447–1459.
55. Hoch MP, Fogel ML, Kirchman DL (1994) Isotope fractionation during ammonium uptake by marine microbial assemblages. *Geomicrobiol J* 12:113–127.
56. Brochier-Armanet C, Boussau B, Gribaldo S, Forterre P (2008) Mesophilic crenarchaeota: Proposal for a third archaeal phylum, the Thaumarchaeota. *Nat Rev Microbiol* 6:245–252.
57. Martens-Habbena W, Berube PM, Urakawa H, de la Torre JR, Stahl DA (2009) Ammonia oxidation kinetics determine niche separation of nitrifying Archaea and Bacteria. *Nature* 461:976–U234.
58. Kuypers MMM, et al. (2001) Massive expansion of marine archaea during a mid-Cretaceous oceanic anoxic event. *Science* 293:92–94.
59. Casciotti KL, Sigman DM, Ward BB (2003) Linking diversity and stable isotope fractionation in ammonia-oxidizing bacteria. *Geomicrobiol J* 20:335–353.
60. Santoro AE, Casciotti KL (2011) Enrichment and characterization of ammonia-oxidizing archaea from the open ocean: Phylogeny, physiology and stable isotope fractionation. *ISME J*, 10.1038/ismej.2011.58.
61. Meckler AN, et al. (2007) Detailed sedimentary N isotope records from Cariaco Basinfor Terminations I and V: Local and global implications. *Global Biogeochem Cy* 21:GB4019.
62. Kuypers MMM, et al. (2003) Anaerobic ammonium oxidation by anammox bacteria in the Black Sea. *Nature* 422:608–611.
63. Meyer KM, Kump LR (2008) Oceanic euxinia in Earth history: Causes and consequences. *Annu Rev Earth Pl Sc* 36:251–288.

Supporting Information

Higgins et al. 10.1073/pnas.1104313109

SI Text

SI Materials and Methods. Sediments were obtained from Ocean Drilling Program Leg 207, Site 1258A, from the Demerara Rise, offshore from modern Surinam. Samples spanned 415–428 m composite depth (mcd). Forty samples were analyzed for bulk $\delta^{15}N_{TN}$, $\delta^{15}N_{kerogen}$, and $\delta^{15}N_{por}$ at approximately 0.5-m spacing. Sampling resolution was higher leading into and coming out of the Oceanic Anoxic Event (OAE), which spanned approximately 422–426 mcd (Table S1).

All reagents used for chromatographic separation were Burdick and Jackson GC^2 grade. The porphyrin standard used was vanadyl-octaethylporphine (Frontier Scientific). Sample preparation followed the methods outlined in (1). Samples were extracted using accelerated solvent extraction (ASE) (Dionex) using 90:10 DCM/MeOH. Total lipid extracts (TLEs) were separated using Flash chromatography (Biotage) using a 12i SIL column (12 mm × 250 mm, 40–63 μm). Porphyrins were eluted into two fractions: fraction 1 (F1), which contains mostly Ni porphyrins, was eluted with 30 mL followed by 15 mL of 1:1 dichloromethane (DCM)/hexane. Fraction 2 (F2), which contains mostly vanadyl (VO) porphyrins, was eluted using two 30 mL aliquots of DCM.

Flash fractions were analyzed using normal-phase (NP-) HPLC (Agilent) with a ZORBAX SIL column (4.6 × 25 mm, 5 μm). The elution program was a 30 min gradient from 100% hexane to 100% ethyl acetate, at 1 mL/min. Absorbance was monitored at 393 and 405 nm, corresponding to absorption maxima of Ni- and VO-porphyrins, respectively. Sample porphyrin concentration was estimated using an empirically derived conversion factor between integrated absorbance and sample [N]. This conversion factor was approximately 8×10^{-4} nmol N $*$ m AU^{-1} $*$ min^{-1} for Ni porphyrins (F1) and approximately 4×10^{-4} nmol N$*$ m AU^{-1} $*$ min^{-1} for VO porphyrins (F2). Each sample was aliquoted into an HPLC vial at a volume estimated to correspond to 50 nmol N, and then injected using the same elution program, with fraction collection programmed to occur at times of absorbance peaks at 393 nm (F1) and 405 nm (F2). For this study, because all sampled horizons contained VO porphyrins, but only some contained Ni porphyrins, only F2 samples were used for isotopic analysis.

Following HPLC collection, samples were oxidized quantitatively to NO_3^- following methods of (1). This was achieved using a two-step oxidation: UV oxidation in quartz tubes, followed by chemical oxidation using $K_2S_2O_8$/NaOH (0.05 mM and 0.15 mM, respectively). Oxidized samples were measured for [NO_3^-] by reduction to NO and measurement of [NO] using a nitric oxide analyzer (Monitor Labs). Samples containing 10 nmol N were analyzed for $\delta^{15}N$ using the denitrifier method (2) using IAEA N3 as a standard.

Samples were analyzed for bulk and kerogen values of $\delta^{15}N$ by EA-IRMS. Rock powder was analyzed for $\delta^{15}N_{TN}$, and ASE-extracted rock powder ("kerogen") was analyzed for $\delta^{15}N_{kerogen}$.

SI Nitrogen Isotopic Records of Sediments, Porphyrins, and Kerogen. We define the onset of the excursion at 426.3 mcd, which corresponds to the first value of $\delta^{13}C_{TOC}$ that is significantly (>2σ) higher than all values deeper in the section (Fig. 1*A*). The first point that marks the end of the excursion is 422.2 mcd. Carbon isotope and total organic carbon (TOC) data are taken from ref. 3, and correspond to the same core used in this study. Data are shown in Table S1.

SI NH_4^+ Upwelling Model. Since all processes that act as sinks for NH_4^+ and NO_3^- are associated with typical kinetic isotope effects (producing isotopically depleted products), generating an isotopically depleted residual DIN pool is difficult. Conventional denitrification results in ^{15}N enrichment of the unused NO_3^-; NH_4^+ oxidation results in ^{15}N enrichment of residual NH_4^+, and under conditions of partial NH_4^+ utilization in assimilatory consumption, fractionation during uptake also results in ^{15}N enrichment of the remaining NH_4^+. The only component of the DIN pool that can become depleted in ^{15}N through these primary effects is NO_2^-, which has an inverse isotope effect associated with nitrification (producing ^{15}N-enriched NO_3^- and leaving behind ^{15}N-depleted NO_2^-) (4). However, it is unlikely that NO_2^- is utilized significantly as a source of nutrient N.

Critically, the above processes do not occur individually or in isolation. ^{15}N-depleted DIN can be produced if these processes are considered as a system that branches at the point of NH_4^+. Because two processes compete for this substrate, the $\delta^{15}N$ values of each product (NO_2^- and biomass) depend on the isotopic fractionation associated with each process (5). The process that has the larger isotope effect generates a more ^{15}N-depleted product. In the case of isotopically depleted biomass associated with OAEs, this would require a larger fractionation associated with NH_4^+ utilization than with NH_4^+ oxidation.

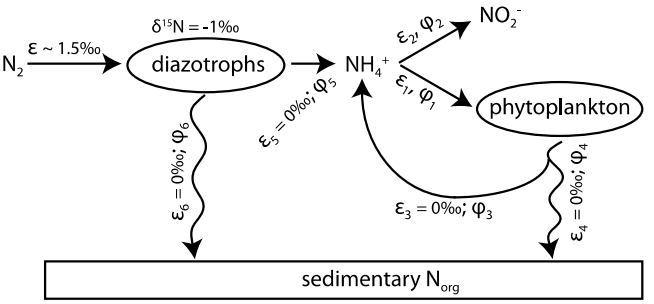

Such a scenario is sketched in the figure above, on which Fig. 2*A* is based. Under conditions of basin-wide anoxia, limited nitrification causes a buildup of NH_4^+ that is derived from organic-matter remineralization in deep waters. NH_4^+ is upwelled into surface waters and fuels primary production. This scenario assumes that NO_2^- is not a source of nutrient N, and that any NO_3^- produced in the aerobic photic zone is not a significant source of nutrient N and ultimately is quantitatively reduced to N_2 in the chemocline. The result is an ocean in which NH_4^+ and N_2 are the only significant bioavailable sources of N. In this model, assuming the only expressed fractionations are ε_{fix} (N_2 fixation), ε_1 (NH_4^+ assimilation) and ε_2 (NH_4^+ oxidation), we can solve for $\delta^{15}N$ values of NH_4^+, NO_2^-, and secondary biomass.

We first set a mass balance around NH_4^+:

$$\delta_{diaz} * \varphi_5 + \delta_{phyt} * \varphi_3 = \varphi_1 * \delta_{phyt} + \varphi_2 * \delta_{NO_2}.$$

Then substitute φ_5:

$$\delta_{diaz} * (\varphi_1 + \varphi_2 - \varphi_3) = (\varphi_1 - \varphi_3) * \delta_{phyt} + \varphi_2 * \delta_{NO_2}.$$

Substitute $\delta_{phyt} = \delta_{NH_4} - \varepsilon_1$ and $\delta_{NO_2} = \delta_{NH_4} - \varepsilon_2$:

$$\delta_{diaz} * (\varphi_1 + \varphi_2 - \varphi_3) = (\varphi_1 - \varphi_3) * (\delta_{NH_4} - \varepsilon_1) + \varphi_2 * (\delta_{NH_4} - \varepsilon_2).$$

Rearrange:

$$\delta_{NH_4} = \delta_{diaz} + \frac{\varphi_1 - \varphi_3}{\varphi_1 + \varphi_2 - \varphi_3} * \varepsilon_1 + \frac{\varphi_2}{\varphi_1 + \varphi_2 - \varphi_3} * \varepsilon_2.$$

Solve for δ_{phyt}:

$$\delta_{phyt} = \delta_{diaz} + \frac{\varphi_1 - \varphi_3}{\varphi_1 + \varphi_2 - \varphi_3} * \varepsilon_1 + \frac{\varphi_2}{\varphi_1 + \varphi_2 - \varphi_3} * \varepsilon_2 - \varepsilon_1.$$

Isotope mass balance for sediments:

$$\delta_{sed} = \frac{\delta_{diaz} * \varphi_6 + \delta_{phyto} * \varphi_4}{\varphi_6 + \varphi_4}.$$

Given the following:

$$f_{remin} = \frac{\varphi_3}{\varphi_1}$$
$$\delta_{diaz} = -1‰$$
$$\%_{cyano} = D = \frac{\varphi_6}{\varphi_4 + \varphi_6}$$
$$f_2 = \frac{\varphi_2}{\varphi_1 + \varphi_2}.$$

If $\varphi_2 = X$ and N_2 fixation flux = 1, then

$$\varphi_6 = (1 - X) * D \qquad \varphi_4 = (1 - X) * (1 - D)$$
$$\varphi_5 = 1 - (1 - X) * D \qquad \varphi_1 = \varphi_2 * \frac{1 - f_2}{f_2}.$$

We substitute the above fluxes into the mass balance around NH_4^+:

$$\varphi_5 + \varphi_3 = \varphi_1 + \varphi_2$$
$$\rightarrow 1 - (1 - X) * D + \varphi_1 * f_{remin} = \varphi_2 * \frac{1 - f_2}{f_2} + \varphi_2$$
$$\rightarrow 1 - (1 - X) * D + \varphi_2 * \frac{1 - f_2}{f_2} * f_{remin} = \varphi_2 * \left(\frac{1 - f_2}{f_2} + 1\right)$$
$$\rightarrow 1 - (1 - X) * D + X * \frac{1 - f_2}{f_2} * f_{remin} = X * \left(\frac{1 - f_2}{f_2} + 1\right)$$
$$\rightarrow\rightarrow X = \frac{D - 1}{\frac{1 - f_2}{f_2} * (f_{remin} - 1) - 1 + D}.$$

Solve for φ_1, φ_3, φ_4, φ_5, φ_6 as a function of X, and use those values to solve for δ_{sed}.

To generate negative $\delta^{15}N$ values of secondary biomass, ε_1 must be $>\varepsilon_2$. Assuming that sedimenting organic matter contains a mixture of material derived from N fixation and the remainder reflects biomass produced from recycled NH_4^+ (similar to today's ocean, but with NH_4^+ substituting for NO_3^-), the $\delta^{15}N$ values of sedimentary organic nitrogen as a function of ε_1, ε_2, φ_2 (fraction nitrification/denitrification), and % contribution of diazotrophic biomass to export production are shown in Fig. 2 *B–D*. These figures assume $\delta_{diazo} = -1‰$ and $f_{remin} = 0.8$. According to this simple model, peak depletions in $\delta^{15}N_{org}$ values occur as the value of $\varepsilon_1 - \varepsilon_2$ increases. Increased contribution of diazotrophic biomass drives average $\delta^{15}N_{org}$ values toward the $\delta^{15}N$ value of nitrogen fixers. Increased contribution of eukaryotic phytoplankton drives average $\delta^{15}N_{org}$ values away from $-1‰$, toward more negative values.

Nitrate utilization cannot be invoked to explain values of sedimentary $\delta^{15}N_{TN} < -2‰$. A model analogous to Fig. 2*A* but written for NO_3^- assimilation ($\varepsilon_{1'}$) vs. denitrification ($\varepsilon_{2'}$) cannot satisfy $\varepsilon_{1'} > \varepsilon_{2'}$. Indeed the positive values for $\delta^{15}N_{NO_3^-}$ in the modern ocean arise because the opposite is true ($\varepsilon_{2'} > \varepsilon_{1'}$). Nitrate assimilation fractionates by approximately 5–10‰ and often is not completely expressed due to quantitative consumption of available NO_3^-. This value is smaller than the minimum approximately 13‰ fractionation associated with denitrification ($\varepsilon_{2'}$) in the water-column, when NO_3^- is not utilized to completion.

We also developed a two-box steady-state model to further clarify the conceptual explanation for depleted sedimentary $\delta^{15}N$ values (Fig. S1). This model, although certainly a great oversimplification of oceanic biological complexity, is meant to test whether a decrease in sedimentary $\delta^{15}N$ values can occur when known nitrogen transformations occur under expected chemical conditions and with expected kinetic isotope fractionations.

The model contains a surface ocean (defined as the photic zone) and a deep ocean. It calculates isotopic values for four nitrogen species (biomass N, NH_4^+, NO_2^-, and NO_3^-) in each box, specifies $\delta^{15}N_{N2}$ of the atmosphere as 0‰, and calculates the $\delta^{15}N$ value of accumulating sediments. The processes modeled are assimilation of NH_4^+ and NO_3^- by biomass (biomass N), remineralization of biomass N to NH_4^+, two-step nitrification ($NH_4^+ \rightarrow NO_2^- \rightarrow NO_3^-$), denitrification ($NO_3^- \rightarrow N_2$), anammox ($NH_4^+ + NO_2^- \rightarrow 2N_2$), and N_2 fixation (the last set as a balanced flux to compensate for all losses).

The model first was optimized to generate output consistent with $\delta^{15}N$ values found in the modern ocean (Fig. S1, blue text values; Table S2). The model rates of nitrogen fixation of approximately 124 Tg N/y, heterotrophic denitrification of approximately 96 Tg N/y (where 80% occurs in sediment), and anammox loss of approximately 18 Tg N/y all are comparable to currently estimated values for these processes (6, 7). The isotopic composition of the resulting simulated N pools depends strongly on the kinetic isotope effects (KIEs) assigned to water-column denitrification, consistent with other models of the modern ocean (8). The model also accurately simulates expansion of regional anoxic zones in an otherwise oxidized ocean circulation system (i.e., the situation of higher values of $\delta^{15}N_{NO_3^-}$).

To run the model for the OAE, we maintained a modern rate of upwelling and the same rate of primary production, but we increased the total rate of denitrification and anammox from approximately 114 to approximately 291 Tg N/y to reflect the driving force for a diazotrophic increase of approximately 2.5×. We presume fully anoxic deep basins are consistent with speciation of most fixed N as NH_4^+ and set the ratio of NH_4^+:NO_2^-:NO_3^- equal to 90:5:5. We then nitrified the upwelling waters such that surface water speciation was 49:2:49. Because the model quantitatively denitrifies downwelling NO_2^- and NO_3^-, we assume that sedimentary denitrification always is negligible. We also increased anammox as a fraction of denitrification between the modern and the OAE scenarios. The OAE scenario therefore primarily alters the proportion of N cycling through processes that use NH_4^+, and in so doing, it generates biomass that has negative values of $\delta^{15}N$ (Fig. S1, green text; boxes 2, 3, and 8). Deep and surface biomass under the OAE scenario have values of −4.4‰ and −5.3‰, respectively, significantly more depleted than in the modern scenario, whereas values of deep NH_4^+ and deep NO_3^- are −1.5‰ and −4.7‰, respectively. Sedimentary $\delta^{15}N$ values in the OAE scenario are −4.4‰, compared to 4.9‰ in the modern scenario.

Since KIEs associated with NH_4^+ assimilation and oxidation are uncertain (see discussion in main text), the same values were used in both ocean scenarios for this exercise (Fig. S1). Culture-based measurements of KIEs associated with NH_4^+ assimilation and oxidation under conditions of low NH_4^+ average 4‰ and 22‰, respectively (9, 10). However, neither value reflects culturing conditions that resemble the chemistry of surface waters in the modern ocean; and likewise, it is impossible to know the true chemistry of the Cretaceous surface ocean. The important outcome of the box model exercise, however, is the relative insensitivity to these choices of values. The model can reproduce observed values of $\delta^{15}N_{TN}$ for both the modern and Cretaceous simply by changing N speciation in accordance with differences in N redox state.

To address this more thoroughly, we conducted sensitivity tests to examine the effects of varying KIEs associated with NH_4^+ oxidation/assimilation, as well as surface water NH_4^+ recycling, enrichment associated with sedimentary diagenesis, and surface water NH_4^+ oxidation/assimilation ratios on sedimentary $\delta^{15}N$ values (Table S3). These tests were done under both the modern and the OAE scenarios. The model generates negative values for $\delta^{15}N_{sed}$ in the OAE scenario when $\varepsilon_{assim} > \varepsilon_{nitrif}$ and surface recycling and/or ammonium oxidation rates are increased. Values of $\delta^{15}N_{sed}$ and are more depleted under smaller values of ε_{nitrif}. Additional sedimentary ^{15}N depletion occurs with the loss of diagenetic ^{15}N enrichment under anoxic sedimentary conditions (11, 12).

The overall finding is that the most important determinant of sedimentary $\delta^{15}N_{TN}$ values appears to be the speciation of nutrient N used by primary producers: N_2, NH_4^+, or NO_3^-. Rates of primary production and upwelling, the total N inventory, and KIEs for enzymatic processes all could be relatively similar during OAEs relative to their values under modern conditions.

1. Higgins MB, Robinson RS, Casciotti KL, McIlvin MR, Pearson A (2009) A method for determining the nitrogen isotopic composition of porphyrins. *Anal Chem* 81:184–192.
2. Sigman DM, et al. (2001) A bacterial method for the nitrogen isotopic analysis of nitrate in seawater and freshwater. *Anal Chem* 73:4145–4153.
3. Erbacher J, Friedrich O, Wilson PA, Birch H, Mutterlose J (2005) Stable organic carbon isotope stratigraphy across Oceanic Anoxic Event 2 of Demerara Rise, western tropical Atlantic. *Geochem Geophy Geosy* 6:Q06010.
4. Casciotti KL (2009) Inverse kinetic isotope fractionation during bacterial nitrite oxidation. *Geochim Cosmochim Acta* 73:2061–2076.
5. Hayes JM (2001) Fractionation of carbon and hydrogen isotopes in biosynthetic processes. *Stable Isotope Geochemistry*, Reviews in Mineralogy and Geochemistry, Vol 43, pp 225–277.
6. Gruber N, Sarmiento JL (1997) Global patterns of nitrogen fixation and denitrification. *Global Biogeochem Cy* 11:235–266.
7. Deutsch C, Sarmiento JL, Sigman DM, Gruber N, Dunne JP (2007) Spatial coupling of nitrogen inputs and losses in the ocean. *Nature* 445:163–167.
8. Brandes JA, Devol AH (2002) A global marine nitrogen isotopic budget: Implications for Holocene nitrogen cycling. *Global Biogeochem Cys* 16:1120.
9. Hoch MP, Fogel ML, Kirchman DL (1992) Isotope fractionation associated with ammonium uptake by a marine bacterium. *Limnol Oceanogr* 37:1447–1459.
10. Santoro AE, Casciotti KL (2011) Enrichment and characterization of ammonia-oxidizing archaea from the open ocean: Phylogeny, physiology and stable isotope fractionation. *ISME J* 5:1796–1808.
11. Altabet MA, Francois R (1994) Sedimentary nitrogen isotopic ratio as a recorder for surface ocean nitrate utilization. *Global Biogeochem Cy* 8:103–116.
12. Gaye-Haake B, et al. (2005) Stable nitrogen isotopic ratios of sinking particles and sediments from the northern Indian Ocean. *Mar Chem* 96:243–255.

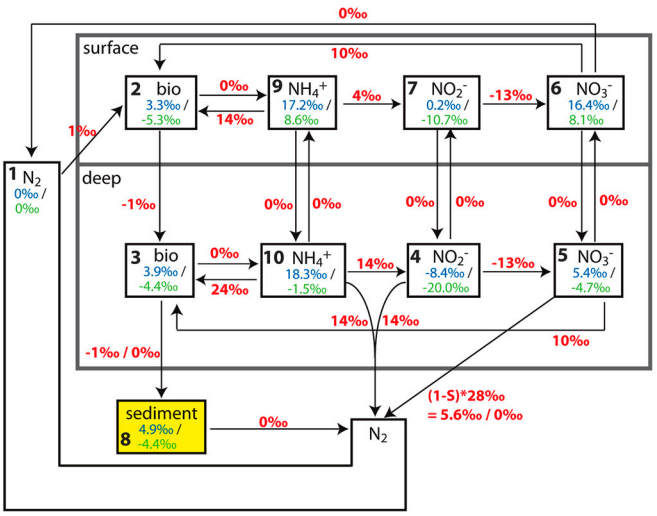

Fig. S1. Results of the 2-Box steady-state model. Values of $\delta^{15}N$ for the modern ocean are shown in blue and for the Cretaceous ocean are shown in green. Values for KIEs (values of ε) are shown in red text next to the flux arrows to which they were applied. Where two ε values are listed, the first indicates the value used for the modern, and the second is the value used in the OAE scenario.

Table S1. Data collected for this study

mcd	$\delta^{15}N_{TN}$	$\delta^{15}N_{ker}$	Raw $\delta^{15}N_{por}$	Blank-corrected $\delta^{15}N_{por}$	$\varepsilon_{ker\text{-}por}$	$\varepsilon_{TN\text{-}por}$
415.52	−0.4 ± 0.6	−1.6	−6.3 ± 0.0	−5.8 ± 0.5	4.2 ± 0.6	5.4 ± 0.8
415.52		−1.6	−7.0 ± 0.4	−6.5 ± 0.6	4.8 ± 0.6	—
416.565	−0.9 ± 0.3	−1.0	−5.4 ± 0.2	−5.0 ± 0.6	4.0 ± 0.6	4.2 ± 0.6
417.23	−1.0 ± 0.2	−1.2	−5.7 ± 0.8	−5.2 ± 0.7	4.0 ± 0.7	—
417.27	−1.0 ± 0.2	−1.2	−6.0 ± 0.0	−5.4 ± 0.4	4.2 ± 0.5	4.4 ± 0.5
417.27	−1.0 ± 0.2	−1.2	−6.0 ± 0.2	−5.5 ± 0.6	4.4 ± 0.6	—
418.005	−1.8 ± 0.2	−2.6	−7.2 ± 0.2	−6.6 ± 0.5	4.1 ± 0.5	4.9 ± 0.5
418.52	−1.3 ± 0.3	−1.6	−5.4 ± 0.1	−4.8 ± 0.5	3.2 ± 0.5	3.5 ± 0.5
419	−1.9 ± 0.7	−2.2	−6.3 ± 0.3	−5.7 ± 0.6	3.5 ± 0.6	3.5 ± 0.6
419.53	−2.2 ± 0.2	−2.6	−5.8 ± 0.8	−5.8 ± 0.9	3.2 ± 0.9	3.6 ± 0.9
420	−2.1 ± 0.3	−2.7	−7.0 ± 0.2	−6.5 ± 0.5	3.8 ± 0.6	4.3 ± 0.6
420.25	−2.1 ± 0.2	−2.8	−7.0 ± 0.4	−6.5 ± 0.6	3.7 ± 0.7	4.4 ± 0.7
421	−1.6 ± 0.1	−1.9	−6.4 ± 0.2	−5.9 ± 0.5	4.0 ± 0.6	4.3 ± 0.6
421.34	−2.4 ± 0.1	−2.9	−7.2 ± 0.1	−6.7 ± 0.4	3.7 ± 0.5	4.3 ± 0.5
421.92	−2.1 ± 0.3	−2.8	−6.8 ± 0.2	−6.3 ± 0.6	3.6 ± 0.6	4.2 ± 0.6
422.05	−2.0 ± 0.4	−2.6	−6.6 ± 0.1	−6.0 ± 0.4	3.4 ± 0.5	3.8 ± 0.5
422.22	−2.2 ± 0.1	−2.6	−7.5 ± 0.2	−6.9 ± 0.5	4.3 ± 0.5	4.7 ± 0.5
422.38	−1.8 ± 0.3	−2.1	−8.0 ± 0.2	−7.5 ± 0.6	5.5 ± 0.6	5.5 ± 0.6
422.51	−2.1 ± 0.1	−2.6	−6.3 ± 0.9	−5.2 ± 0.8	2.6 ± 0.8	3.2 ± 0.8
422.67	−2.5 ± 0.2	−2.6	−7.4 ± 0.3	−6.9 ± 0.5	4.3 ± 0.6	4.4 ± 0.6
422.965	−1.8 ± 0.2	−2.0	−6.7 ± 0.1	−6.2 ± 0.5	4.2 ± 0.5	4.4 ± 0.5
423.256	−1.4 ± 0.1	−1.7	−5.4 ± 0.3	−4.8 ± 0.5	3.1 ± 0.6	3.4 ± 0.6
423.56	−0.9 ± 0.2	−1.3	−5.0 ± 0.4	−4.7 ± 1.0	3.4 ± 1.0	3.7 ± 1.0
423.87	—	—	−6.9 ± 0.0	−6.4 ± 0.5	—	—
424.01	−1.2 ± 0.2	−1.5	−5.6 ± 0.0	−4.9 ± 0.4	3.4 ± 0.5	3.7 ± 0.4
424.32	−2.0 ± 0.2	−2.9	−5.7 ± 0.4	−5.2 ± 0.7	2.3 ± 0.8	3.2 ± 0.8
424.595	−1.7 ± 0.2	−2.1	−6.7 ± 0.3	−6.2 ± 0.6	4.1 ± 0.6	4.4 ± 0.6
424.885	−0.4 ± 0.3	−0.9	−5.1 ± 0.2	−4.5 ± 0.5	3.6 ± 0.6	4.1 ± 0.5
425.325	−2.0 ± 0.1	—	−6.4 ± 0.3	−5.9 ± 0.6	—	3.9 ± 0.6
425.68	−1.4 ± 0.4	−2.4	−6.8 ± 0.4	−6.3 ± 0.6	3.9 ± 0.6	4.6 ± 0.6
425.83	−0.8 ± 0.1	−0.8	−5.3 ± 0.1	−4.8 ± 0.6	4.0 ± 0.6	3.9 ± 0.6
426.15	−2.0 ± 0.2	−1.5	−5.9 ± 0.0	−5.3 ± 0.4	3.8 ± 0.5	3.3 ± 0.5
426.28	−0.7 ± 0.1	−1.4	−5.7 ± 0.6	−5.1 ± 0.8	3.8 ± 0.8	4.4 ± 0.8
426.455	−0.9 ± 0.3	−1.3	−6.3 ± 0.1	−5.9 ± 0.6	4.6 ± 0.7	5.0 ± 0.7
426.58	−0.7 ± 0.2	−1.3	−5.8 ± 0.4	−5.3 ± 0.6	4.0 ± 0.7	4.6 ± 0.7
426.735	−1.8 ± 0.2	−1.8	−6.7 ± 0.4	−6.2 ± 0.6	4.4 ± 0.6	4.4 ± 0.6
427.03	−1.8 ± 0.5	−2.2	−6.2 ± 0.6	−5.6 ± 0.9	3.4 ± 1.0	4.0 ± 1.0
427.18	−1.9 ± 0.2	−2.1	−6.1 ± 0.6	−5.6 ± 0.7	3.5 ± 0.7	3.7 ± 0.7
427.35	—	—	−4.7 ± 0.2	−4.1 ± 0.5	—	—
427.52	−0.5 ± 0.3	−1.2	−6.6 ± 0.2	−6.2 ± 0.7	5.0 ± 0.7	5.6 ± 0.7
427.78	−1.4 ± 0.1	−1.3	−5.3 ± 0.3	−4.7 ± 0.6	3.4 ± 0.6	3.4 ± 0.6
428.095	−0.4 ± 0.1	−0.4	−5.8 ± 0.6	−5.3 ± 0.7	4.9 ± 0.7	4.9 ± 0.7
428.56	−0.1 ± 0.4	−0.4	−7.1 ± 0.2	−6.5 ± 0.5	6.1 ± 0.5	6.1 ± 0.5
434.03	−1.8 ± 0.5	−2.3	−9.0 ± 0.0	−8.6 ± 0.6	6.3 ± 0.6	6.8 ± 0.8
434.73	−2.1 ± 0.1	−2.3	−8.0 ± 0.1	−7.4 ± 0.4	5.1 ± 0.5	5.3 ± 0.4

All $\delta^{15}N$ values are shown $\pm 1\sigma$, and ε values are shown with fully propagated errors. Blank-corrected $\delta^{15}N_{por}$ data reflect a blank with $\delta^{15}N$ value of $0 \pm 10‰$, and Rayleigh fractionation associated with incomplete oxidation of up to 0.7‰ (1).

Table S2. Parameter values for modern and OAE-type oceans

Variable	Note	Definition	Value (modern)	Value (OAE)
NPP	in 10^{15} mol/y	export production	0.075	0.075
Vs	in 10^{15} m^3	surface volume	105	105
Vd	in 10^{15} m^3	deep volume	1421	1421
U	in 10^{15} m^3/y	upwelling	1.95	1.95
INVs	in 10^{15} mol	surface N inventory	0.125	0.125
INVd	in 10^{15} mol	deep N inventory	49.875	49.875
NH_4s	fraction	% NH_4^+ in surface	**4.28E–4**	**0.49**
NO_2s	fraction	% NO_2^- in surface	**4.28E–5**	**0.02**
NH_4d	fraction	% NH_4^+ in deep	**4.28E–4**	**0.9**
NO_2d	fraction	% NO_2^- in deep	**4.28E–5**	**0.05**
m_{atm}	moles	N atmosphere	**1E9**	**1E9**
$m_{surfbio}$	moles	N-surface bio	0.001	0.001
$m_{deepbio}$	moles	N-deep bio	0.01	0.01
m_{sedN}	moles	N sediments	100	100
A	—	$anammox_{NH_4\to N_2}/(deep_{NH_4\to NO_2} + anammox_{NH_4\to N_2})$	**0.0085**	**0.15**
S	—	$denit_{sed}/(denit_{sed} + denit_{water})$	**0.8**	**1**
B	—	N burial/NPP	0.01	0.01
Rec	—	surface recycling = $surf_{bio\to NH_4}$/export	**9**	**13.5**
Ch	—	$deep_{NH_4\to bio}/deep_{NH_4\to NO_2}$	0.05	0.05
Aos	—	$surf_{NH_4\to NO_2}/surf_{NH_4\ fluxin}$	**0.01875**	**0.03**

Table S3. Sensitivity analysis

NH_4^+ Fractionations	Rec	Sediment enrichment (‰)	Modern $\delta^{15}N_{sed}$ (‰)	OAE $\delta^{15}N_{sed}$ (‰) Aos = 0.01875	OAE $\delta^{15}N_{sed}$ (‰) Aos = 0.03
Surface:	9	1	5.7	13.6	13.2
ε_{assim} = 4‰; ε_{nitrif} = 22‰	—	0	4.8	12.6	12.2
Deep:	13.5	1	5.7	13.4	13.0
ε_{assim} = 4‰; ε_{nitrif} = 22‰	—	0	4.8	12.4	12.0
Surface:	9	1	5.5	−2.5	−4.5
ε_{assim} = 14‰; ε_{nitrif} = 4‰		0	4.6	−3.4	−5.4
Deep:	13.5	1	5.5	−4.1	−6.2
ε_{assim} = 14‰; ε_{nitrif} = 4‰	—	0	4.6	−5.0	−7.2
Surface:	9	1	4.9	1.3	−1.3
ε_{assim} = 24‰; ε_{nitrif} = 14‰	—	0	4.0	0.4	−2.2
Deep:	13.5	1	4.9	−0.8	−3.5
ε_{assim} = 24‰; ε_{nitrif} = 14‰	—	0	3.9	−1.7	−4.5
Surface:	9	1	**4.9**	1.4	−1.2
ε_{assim} = 14‰; ε_{nitrif} = 4‰	—	0	4.0	0.5	−2.2
Deep:	13.5	1	**4.9**	−0.7	−3.5
ε_{assim} = 24‰; ε_{nitrif} = 14‰	—	0	3.9	−1.6	**−4.4**

Sedimentary $\delta^{15}N$ values from Fig. S1 are shown in bold.